Study of critical behavior in concrete during curing by application of dynamic linear and nonlinear means

Jean-Christoph Lacouture[a]
*Laboratoire Environnement et Développement, Université D. Diderot, Tour 33-43, Case courrier 7087,
2 Place Jussieu, 75251 Paris Cedex, France*

Paul A. Johnson[b]
Geophysics, MS D443, Los Alamos National Laboratory, Los Alamos, New Mexico 87545

Frederic Cohen-Tenoudji[c]
*Laboratoire Environnement et Développement, Université D. Diderot, Tour 33-43, Case courrier 7087,
2 Place Jussieu, 75251 Paris Cedex, France*

The monitoring of both linear and nonlinear elastic properties of a high performance concrete during curing is presented by application of compressional and shear waves. To follow the linear elastic behavior, both compressional and shear waves are used in wide band pulse echo mode. Through the value of the complex reflection coefficient between the cell material (Lucite) and the concrete within the cell, the elastic moduli are calculated. Simultaneously, the transmission of a continuous compressional sine wave at progressively increasing drive levels permits us to calculate the nonlinear properties by extracting the harmonics amplitudes of the signal. Information regarding the chemical evolution of the concrete based upon the reaction of hydration of cement is obtained by monitoring the temperature inside the sample. These different types of measurements are linked together to interpret the critical behavior. © *2003 Acoustical Society of America.*
[DOI: 10.1121/1.1543927]

PACS numbers: 43.25.Zx, 43.25.Ba, 43.25.Ts, 43.35.Zc [MFH]

I. INTRODUCTION

Concrete, especially Ultra High Performance Concrete (UHPC), is well known to be a complex, multiscale material.[1] The physical properties of concrete evolve significantly during curing, experiencing a phase change, a critical behavior, from the liquid to solid state. The hardening of concrete caused by the reaction of hydration of the cement is a well-studied process[2] and there are many papers dealing with the linear elastic properties of concrete during curing.[3,4] Furthermore, it is known that hardened concrete shows nonlinear properties[5] related in some manner to the presence of microcracking. We are not aware of any studies that monitor both the linear and dynamic nonlinear elastic parameters through a phase change. Nonlinear techniques have the potential to help us unravel the complex physical property changes that take place during a phase change. Concrete is a complex and interesting candidate for study because the phase change takes place over several hours and therefore one can probe the material many times during the change.

This paper begins with a description of the experimental configuration, followed by a description of experimental results, discussion, and conclusions.

II. EXPERIMENTAL PROCEDURE

A cubic-shaped volume $16 \times 16 \times 16$ cm^3 constructed of wooden walls and a base of Lucite is used for the experiment (Fig. 1). High Performance Reactive Powder Concrete composed of Portland cement, thin sand, silica fume, water, and superplasticizer (Tables I and II), is poured into the box, and the monitoring commences immediately. Two wide band piezoelectric transducers of 500 kHz central frequency, are attached to the Lucite base of the experiment cell. One transducer generates compressional and the other shear waves. Both transducers are operated in pulse echo mode. From the measured reflection coefficients and the density, we can calculate the elastic moduli of the concrete (see below) and follow their evolution with time. In order to obtain the nonlinear response, we transmit pure-tone compressional waves at 8 kHz across the sample at 20 successively increasing amplitudes. The piezoceramic (PZT) emitter and receiver are driven at 8 kHz, far from their natural resonant frequency (100 kHz and 200 kHz, respectively) and placed in direct contact with the concrete through holes in the cell walls. We monitor the amplitudes of harmonics in the transmitted signal as a function of the amplitude of the fundamental. In order to avoid interfering effects, the linear and nonlinear measurements are performed at successively different times over the duration of the experiment. That is, the reflection coefficient measurement is conducted, and following this, the nonlinear transmission data are collected, and so on at 5 min intervals. Data are stored and analyzed on the computer. The

[a]Electronic mail: lacoutur@ccr.jussieu.fr
[b]Electronic mail: paj@lanl.gov
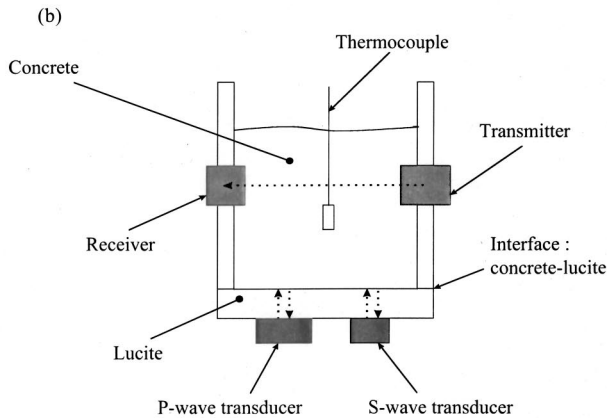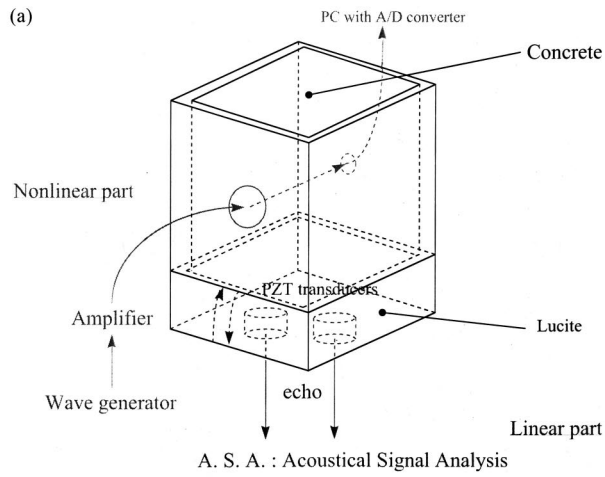[c]Electronic mail: tenoudji@ccr.jussieu.fr

FIG. 1. (a) Bird's-eye view of experimental container showing location of transducers. (b) side view of experimental container. The nonlinear signals are obtained from the waves traversing the box at its midpoint. The wavespeeds are obtained from the reflection coefficients of the *P*- and *S*-waves between the Lucite base and the concrete shown at the container base.

temperature is monitored using a thermocouple embedded in the sample and the ambient temperature is measured with a separate thermocouple.

III. THEORETICAL CONSIDERATIONS

A. Linear elastic moduli

The Young's modulus E and Poisson's ratio v are calculated from the reflection coefficient of longitudinal and shear waves. In an homogeneous medium of density ρ, the wave equation of the displacement U in one dimension x is given by

TABLE I. Cement paste composition.

Component	Density	Dry mass ratio (normalized to cement)	Granulometry (μm)
HTS cement	3.17	1	20
BE31 sand	2.65	1.1	310
MST fume silica	2.27	0.25	0.2
Mapei X404 superplasticizer	1.1	0.011	
Water	1	0.213	

TABLE II. Chemical composition of HTS cement (%).

	HTs cement
$C_2S(3CaOH, SiO_2)$	62–64
$C_2S(2CaOH, SiO_2)$	18–21
$C_2A(3CaOH, Al_2O_3)$	3.8–4.4
$C_4AF(4CaOH, Al_2O_3, Fe_2O_3)$	6.5–7.4

$$\rho \frac{\partial^2 U}{\partial t^2} = M \frac{\partial^2 U}{\partial x^2}, \tag{1}$$

where $M = \lambda + 2\mu$ for longitudinal waves and $M = \mu$ for shear waves, with λ and μ being the Lamé coefficients. In the case of a viscoelastic material M is complex. For harmonic waves, Eq. (1) becomes

$$-\rho \omega^2 U = -M k^2 U, \tag{2}$$

where k is the wave number,

$$\frac{\rho \omega^2}{M} = k^2. \tag{3}$$

Writing $k = k' + ik''$, the phase velocity is given by

$$c = \frac{\omega}{k'}. \tag{4}$$

The stress amplitude reflection coefficient is given by

$$r = \frac{z_2 - z_1}{z_2 + z_1}, \tag{5}$$

where z_1 is the acoustic impedance of the first medium, here the Lucite, and z_2 is the acoustic impedance of the second medium, the concrete.

The impedance is given by

$$z = \sqrt{\rho M}. \tag{6}$$

In the frequency range 100 kHz–600 kHz, the acoustic impedance z_1 of the Lucite remains mostly real. The values are $z_1 = 2 \times 10^6$ Rayl for longitudinal waves and $z_1 = 10^6$ Rayl for shear waves. It is observed that the impedance of the concrete z_2 happens to be highly complex at certain stages of the cure.

The complex reflection coefficient r is obtained in the frequency domain by applying a Fourier transformation (at 300 kHz) of the reflected pulse at the interface concrete-Lucite, normalized in modulus and phase by the amplitude of a air-air reflected signal, as reference. The value of z_2 is calculated with the assumption of an approximately constant concrete density of $\rho = 2.1.10^3$ kg/m^3.

The shear and compressional phase velocities c_s and c_p are evaluated using relations (6) and (4). In the following, the medium is considered as homogeneous. In this case the Young's modulus E and Poisson's ratio v are given by

$$E = 2\rho c_s^2 (1+v) \quad \text{and} \quad v = \frac{\left(1 - 2\frac{c_s^2}{c_p^2}\right)}{2\left(1 - \frac{c_s^2}{c_p^2}\right)}. \tag{7}$$
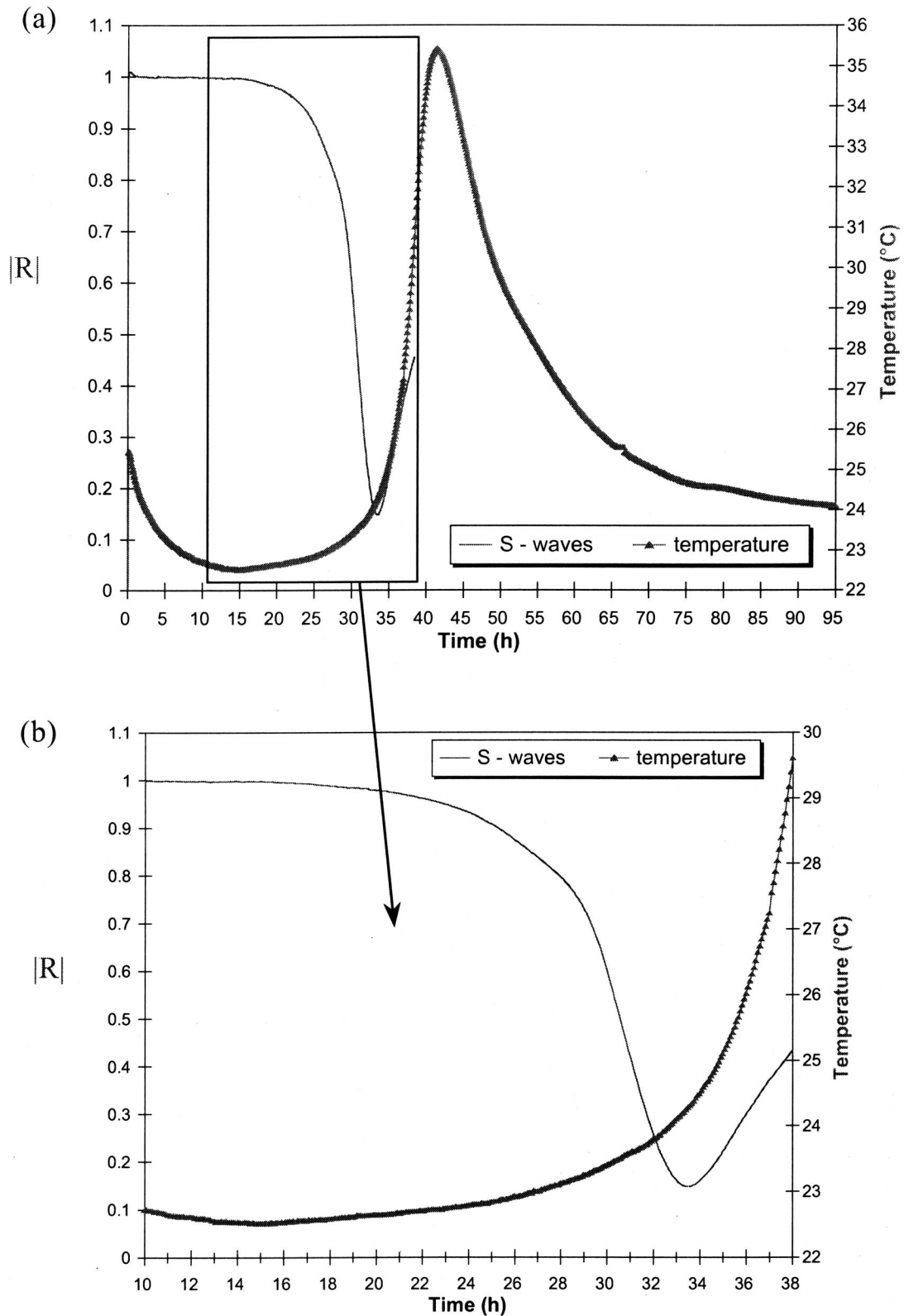
(a)

(b)

FIG. 2. Shear wave reflection coefficient and temperature in the sample between (a) 0 and 95 h (b) 10 and 38 h. The shear and compressional wave reflection coefficients lead to the calculation of the velocities and the elastic moduli.

It is clear that in its initial stage, the concrete has almost no shear elasticity, being fluid. The shear wave velocity is therefore zero. In consequence, the early values of the Young's modulus are zero, and the Poisson's ratio equals 0.5. The hardening will manifest itself by the increasing values of the Young's modulus and a decrease of the Poisson's ratio toward 0.2 approximately when the concrete has hardened.
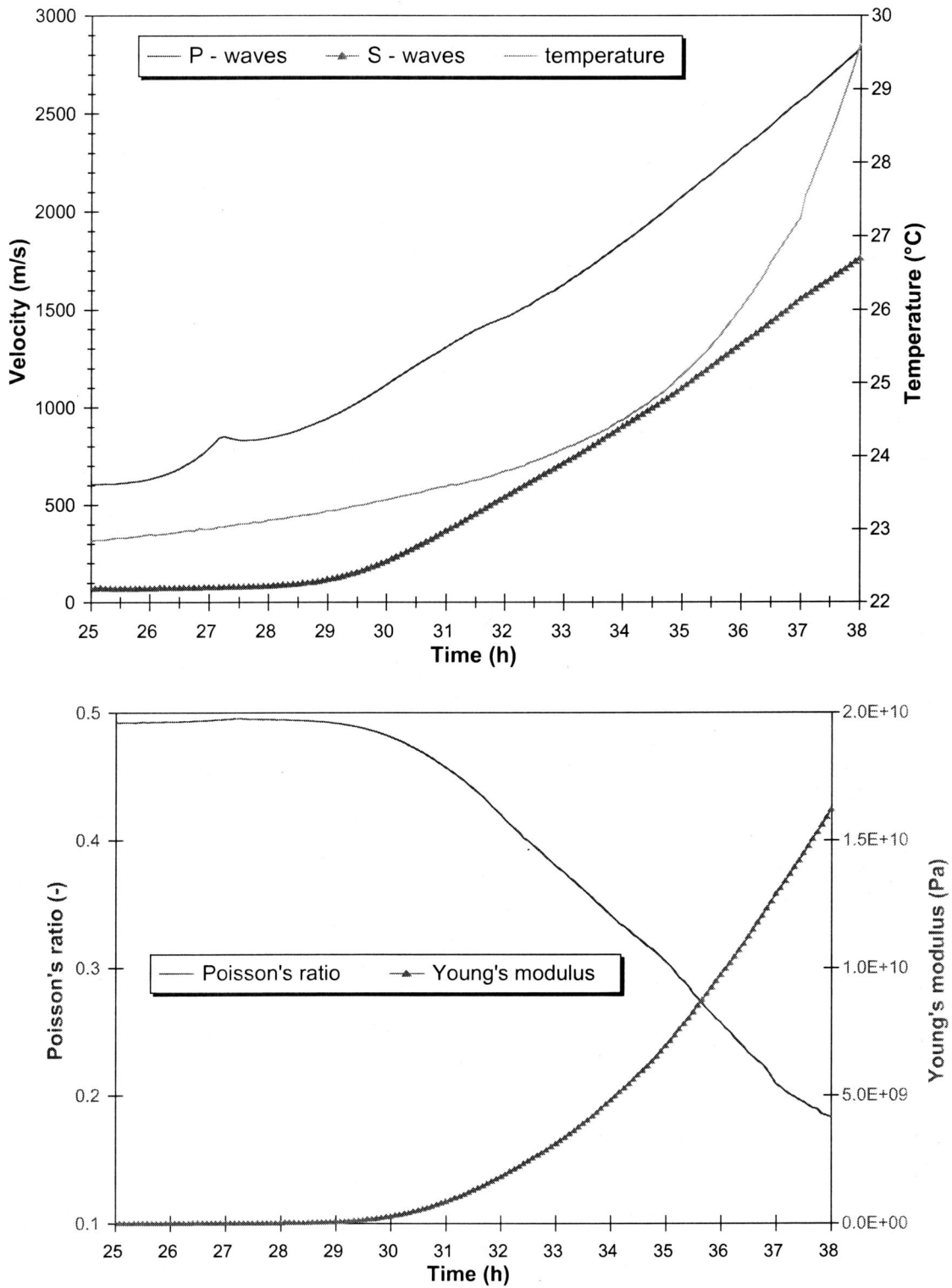
FIG. 3. (a) Velocities and temperature between 25 and 38 h. (b) Young's modulus and Poisson's ratio between 25 and 38 h.

B. Nonlinear elastic moduli

The nonlinear moduli are extracted by using the Preisach-Mayergoyz[6,7] space model of Guyer and McCall.[8–10] This model tells us that, in one dimension, the nonlinear contribution to the modulus can be written

$$k(x,t) = \beta \varepsilon + \ldots - \alpha [\Delta \varepsilon + \text{sign}(\varepsilon)\varepsilon], \tag{8}$$

where β is the "classical" second order nonlinear parameter

(Landau type[11]), and α is the "nonclassical" nonlinear parameter that describes hysteresis in the stress–strain relation. β and α can be calculated with the assumption that the measurements reflect a value proportional to acceleration,[12]

$$\beta \propto \frac{c_p^2 A_2}{(A_1)^2} \quad \text{and} \quad \alpha \propto \frac{c_p^2 A_3}{(A_1)^2}, \tag{9}$$

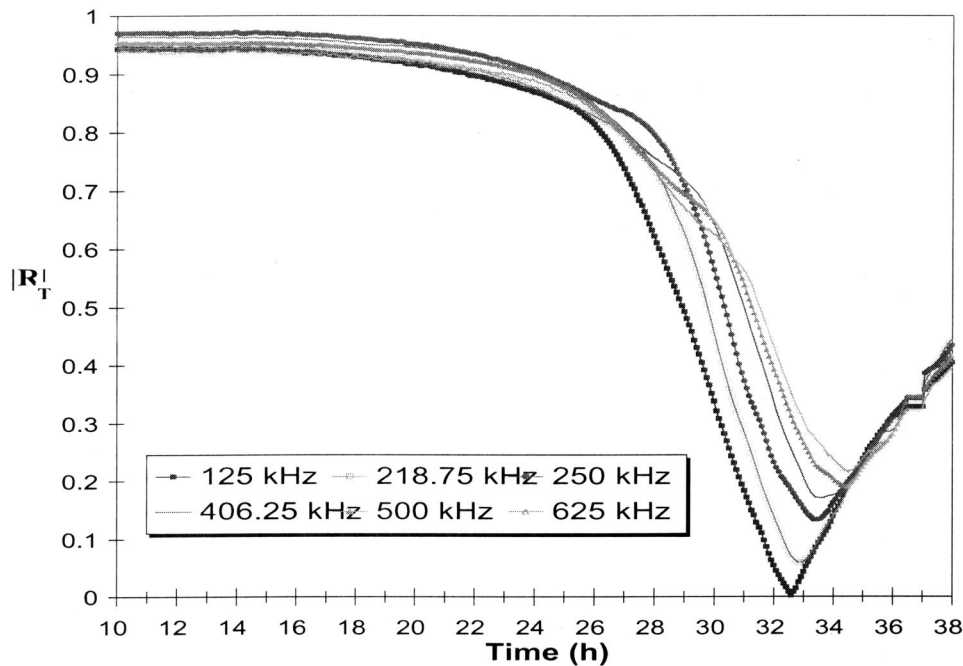Lacouture *et al.*: Monitoring of critical behavior in concrete

FIG. 4. Shear wave reflection coefficient for different frequencies.

where c_p is the compressional wave velocity, A_2 and A_3 are the amplitudes of the second and third harmonics, respectively, and A_1 is the amplitude of the fundamental (input wave), all measured at the detector. By plotting the fundamental wave amplitude versus the harmonic amplitudes at successively larger amplitudes, one can extract the nonlinear coefficients by fitting the data.

IV. RESULTS AND ANALYSIS

Figure 2 shows the temperature measured within the interior of the sample and the shear wave reflection coefficient measured at the base of the sample as described above, as a function of time during the experiment. Due to the progressive shrinkage of the material during curing, a disbonding of the transducers occurs at approximately 38 h after mixing (this is a problem we are currently addressing in order to study the behavior for longer periods of time). The primary chemical reaction begins at approximately 20 h as evidenced by the slope change in the temperature curve. Figure 3(a) shows the compressional (P) and shear (S) wave velocities, and the temperature, as a function of time between 25 and 38 h. Figure 3(b) shows Young's modulus and Poisson's ratio versus time, calculated from the reflection coefficient shown in the previous figure (Fig. 2). It is at this time that isolated solid regions begin to form in the material, however, the material remains in a primarily fluid state until about 29 h, as seen more clearly in the behavior of the moduli in Fig. 3(b) where the Young's modulus remains zero and the Poisson's ratio remains at 0.5. The correlations between the steep rise in temperature shown in Fig. 3 and the minimum in the reflection coefficient shown in Fig. 2 have been studied previously.[4] As seen in Fig. 4, a frequency effect is noticeable in the beginning of the cure starting at approximately 26 h. The acoustic impedance is larger at higher frequencies and the minimum shifts to later time with higher frequency. Full connection takes place at approximately 36–38 h slightly

before the large thermal peak where the curves of the shear wave reflection coefficient for the different frequencies rejoin together (Fig. 4).

In the nonlinear portion of the experiment (Fig. 5), the transmission of the wave is possible only after 23 h, meaning that the fluid material entirely dissipates the wave before this time. The signal can be measured beginning at this time, but it is not until hour 28 that the second harmonic data are reliable, and at hour 30 for the third harmonic data (Fig. 5) corresponding to the rise of the Young's modulus from zero and the decrease of the Poisson's ratio from 0.5 (Fig. 3). We base our reliability on the power law dependence between the fundamental, and second and third harmonic amplitudes. According to Eq. (9) above from the P-M space model, the power law relation should be two in both cases. Noisy harmonic data with indefinable slopes are observed until the times noted above. Figure 5 illustrates several harmonic data sets taken at various times in the experiment. We show data sets taken during the fluid phase (bottom), during partial connection (top left) and when full connection takes place (top right). In all cases, at low drive levels the harmonics lie in the noise, and emerge at decreasing amplitude levels during the curing process. Figure 6(a) shows us only the reliable harmonic dependencies obtained throughout the experiment. In Fig. 6(a) are plotted the variation with time of the power law coefficient of the second and third harmonic amplitude dependences versus the amplitude of fundamental after 28 h. We observe a slope of approximately 2 beginning at hour 28 (A_{2f}) and 30 (A_{3f}). The data are noisy and the error bars indicate this, but the mean values are approximately 2. We believe that the observed dependence differs slightly from two because of the perturbation caused by resonances within the cell. As the experiments are being performed in a continuous sinusoidal excitation mode, a stationary wave within the cell is possible. This effect is less pronounced in the early part of the cure when the attenuation is more pronounced and
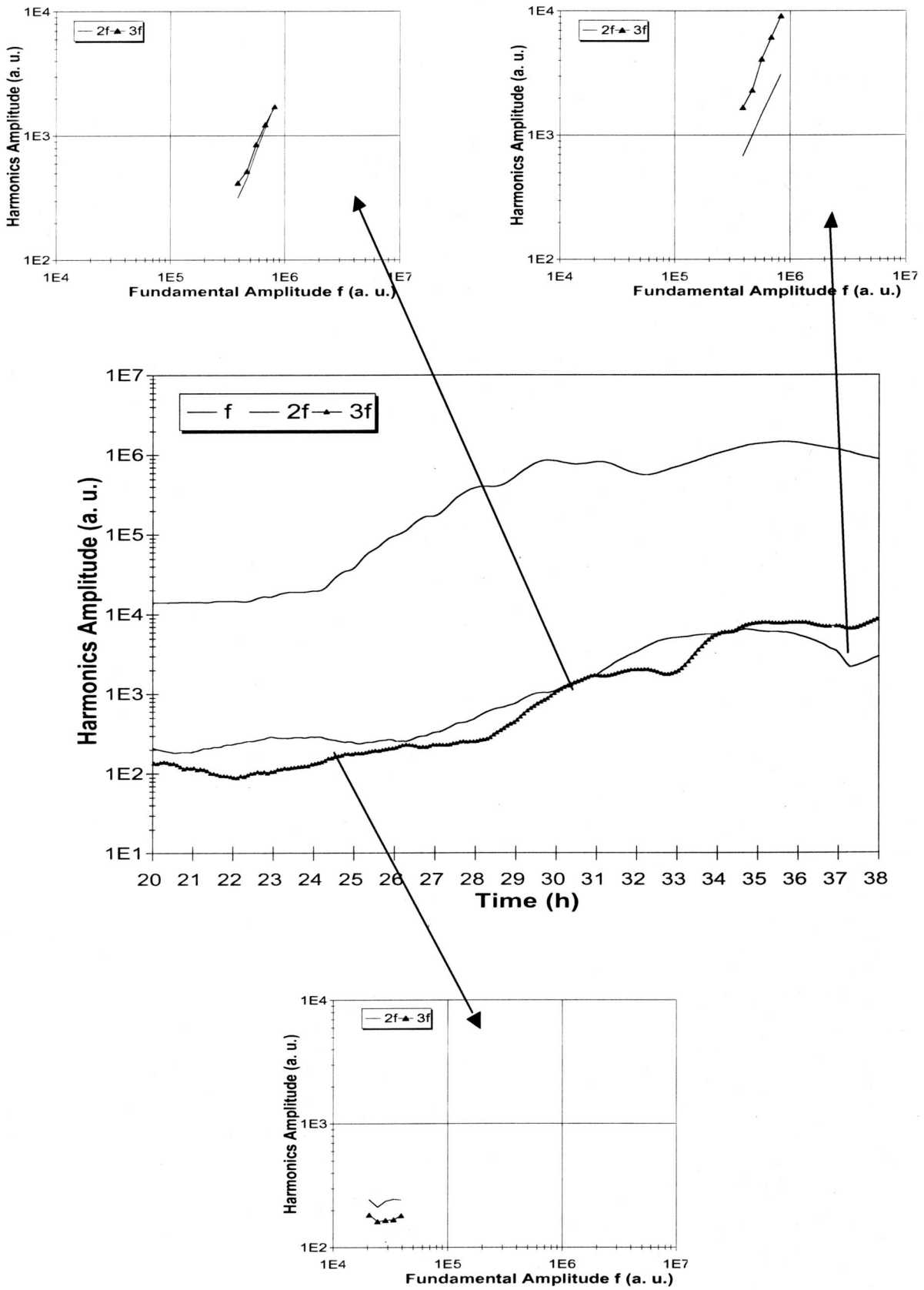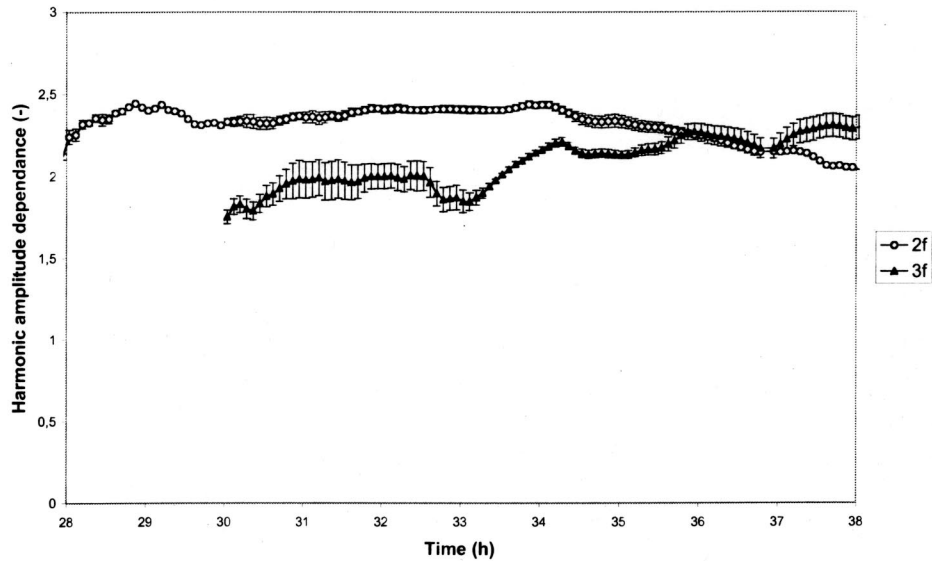
FIG. 5. Harmonic versus fundamental amplitudes.

the multiple reflected signals at the interfaces are small. As the attenuation decreases during the cure and the amplitude of the transmitted signal increases, the effect may become significant as can be seen on the oscillations on the ampli-

tude of the fundamental. The slope of two in the harmonic amplitude dependence for the second and third harmonic indicates that we are in a nonlinear, nonclassical material. Classical nonlinear materials would show a third harmonic
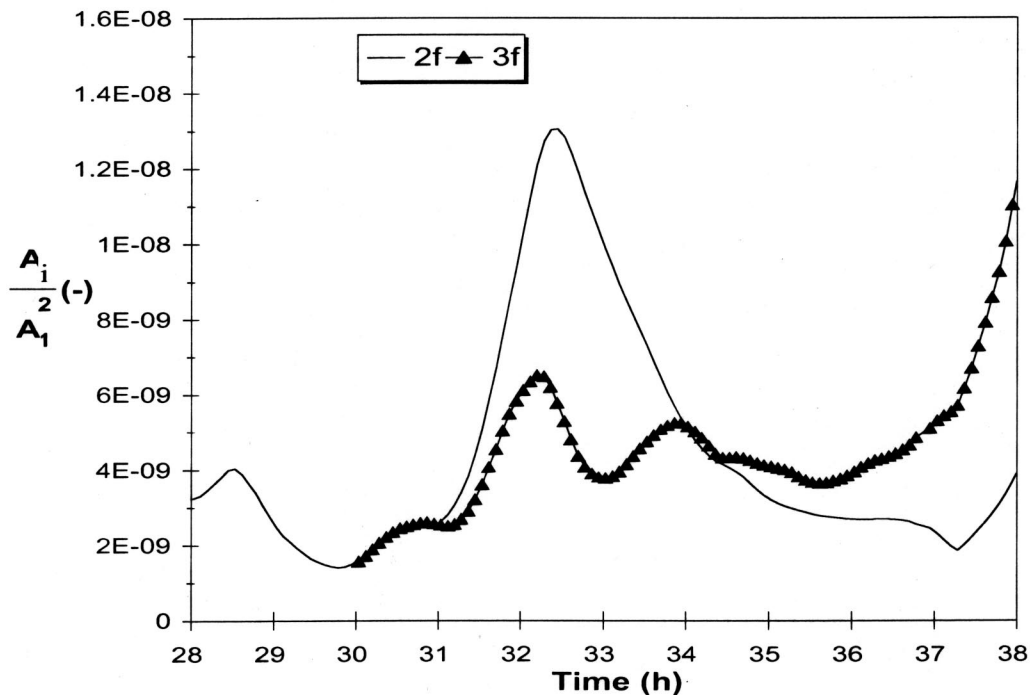
(a)

(b)

FIG. 6. (a) Harmonic amplitude dependence between 28 and 38 h. (b) Nonlinear coefficients between 28 and 38 h.

amplitude proportional to the cube of the fundamental amplitude. Thus we can estimate the nonlinear parameters $A_i/(A_1)^2$ of Eq. (9) that are proportional to nonlinear coefficients α and β of Eq. (8). The results are shown in Fig. 6(b). These are relative values of the nonlinear coefficients because we did not collect calibrated accelerations.

Thus, we can try to link the linear and nonlinear data during curing. From the monitoring of the reflection coefficient, we can see the changes in the mechanical state

of the concrete with the different points in time in the thermal evolution like percolation point or points of connection of the different type of particles. These effects start at the percolation threshold that we assume to be at about 25 h. This point corresponds at the beginning of the thermal peak in the temperature curve [Fig. 2(a)] and to the beginning of a decrease in the shear modulus reflection coefficient in the shear wave reflection coefficient curves (Fig. 4) and in the harmonic amplitude versus time (Fig. 5) where we ob-

J. Acoust. Soc. Am., Vol. 113, No. 3, March 2003

Lacouture *et al.*: Monitoring of critical behavior in concrete   1331

serve the beginning of the rise of the fundamental amplitude. During the thermal peak and the connection of particles in the material, we see a corresponding peak in the nonlinear parameters [Fig. 6(b)] that terminates at the point of the connection of the largest particles that is given by the linear part of the experiment corresponding to the coalescing of the reflection coefficient for different frequencies (Fig. 4).

V. CONCLUSIONS

By monitoring temperature, linear and nonlinear elastic properties, we can infer much regarding the evolution of the concrete during curing. The evolution of the reaction of hydration with the measure of the heat released informs us about the chemical behavior of the material in the experiment. The evolution of the reflection coefficient and moduli provide information about the mechanical state of the concrete including the liquid–solid phase change during the curing.

From monitoring harmonics we also see the phase change through the nonlinear coefficients. Before the thermal peak, in the liquid state, harmonics cannot be seen. These effects start at the percolation point where we notice the beginning of the harmonics generation and a nonclassical, nonlinear dependency. We observe a correlation between nonlinear response and linear response that relates to a known microstructure evolution of the connection of particles in the material. We relate the phase change with the thermal peak. We see that peaks in the nonlinear parameters linked to the nonlinear coefficients end at the point of the connection of the largest particles, as is given by the linear elastic results of the experiment (the reflection coefficient). The results indicate that the concrete is a nonclassical hysteretic elastic nonlinear material, like rock, some metals and ceramics.[13]

[1] C. Vernet, J. Lukasik, and E. Prat, "Nanostructure, porosity, permeability and diffusivity of ultra-high performance concrete," in *Proceedings of Intern. Symp. on HPC and RPC*, edited by P. C. Aïtcin *et al.* (RILEM Publisher, Sherbrooke, 1998), Vol. 3, pp. 17–35.

[2] G. De Schutter and L. Taerwe, "Specific heat and thermal diffusivity of hardening concrete," Cem. Concr. Res. **25**, 593–604 (1995).

[3] A. Boumiz, C. Vernet, and F. Cohen Tenoudji, "Mechanical properties of cement pastes and mortars at early ages: Evolution with time and degree of hydration," Adv. Cem. Based Mater. **3**, 94–106 (1996).

[4] V. Morin, F. Cohen Tenoudji, P. Richard, A. Feylessoufi, and C. Vernet, "Ultrasonic spectroscopy investigation of the structural and mechanical evolutions of reactive powder concretes," *Proceedings of Intern. Symp. on HPC and RPC*, edited by P. C. Aïtcin *et al.* (RILEM Publisher, Sherbrooke, 1998), Vol. 3, pp. 119–126.

[5] P. A. Johnson, "The new wave in acoustic testing," Mater. World **7**, 544–546 (1999).

[6] F. Preisach, Z. Phys. **94**, 277–302 (1935).

[7] I. D. Mayergoyz, "Hysteresis models from the mathematical and control theory point of view," J. Appl. Phys. **57**, 3803–3805 (1985).

[8] K. R. Mccall and R. A. Guyer, "Equation of state and wave propagation in hysteretic nonlinear elastic materials," J. Geophys. Res. **99**, 23887–23897 (1994).

[9] R. A. Guyer and K. R. Mccall, "Hysteresis, discrete memory and nonlinear wave propagation in rock," Phys. Rev. Lett. **74**, 3491–3494 (1995).

[10] K. R. Mccall and R. A. Guyer, "A new theoretical paradigm to describe hysteresis, discrete memory and nonlinear elastic wave propagation in rock," Nonlinear Processes in Geophysics **3**, 89–101 (1996).

[11] L. D. Landau and E. M. Lifshitz, *Theory of Elasticity*, 3rd ed. (Pergamon, Oxford, England, 1986).

[12] K. E-A. VanDenAbeele, P. A. Johnson, R. A. Guyer, and K. R. McCall, "On the quasi-static treatment of hysteretic nonlinear response in elastic wave propagation," J. Acoust. Soc. Am. **101**, 1885–1898 (1997).

[13] R. A. Guyer and P. A. Johnson, "Nonlinear mesoscopic elasticity: Evidence for a new class of materials," Phys. Today **52**, 30–35 (1999).